



Estimation of US
urban NO_x emissions
from OMI

Z. Lu et al.

This discussion paper is/has been under review for the journal Atmospheric Chemistry and Physics (ACP). Please refer to the corresponding final paper in ACP if available.

Emissions of nitrogen oxides from US urban areas: estimation from Ozone Monitoring Instrument retrievals for 2005–2014

Z. Lu¹, D. G. Streets¹, B. de Foy², L. N. Lamsal^{3,4}, B. N. Duncan⁴, and J. Xing⁵

¹Energy Systems Division, Argonne National Laboratory, Argonne, IL 60439, USA

²Department of Earth and Atmospheric Sciences, Saint Louis University, St. Louis, MO 63108, USA

³Goddard Earth Sciences Technology and Research, Universities Space Research Association, Columbia, MD 21046, USA

⁴NASA Goddard Space Flight Center, Greenbelt, MD 20771, USA

⁵US Environmental Protection Agency, Research Triangle Park, NC 27711, USA

Received: 25 March 2015 – Accepted: 11 May 2015 – Published: 28 May 2015

Correspondence to: Z. Lu (zlu@anl.gov)

Published by Copernicus Publications on behalf of the European Geosciences Union.

Title Page

Abstract

Introduction

Conclusions

References

Tables

Figures



Back

Close

Full Screen / Esc

Printer-friendly Version

Interactive Discussion



Abstract

Satellite remote sensing of tropospheric nitrogen dioxide (NO_2) can provide valuable information for estimating surface nitrogen oxides (NO_x) emissions. Using an exponentially-modified Gaussian (EMG) method and taking into account the effect of wind on observed NO_2 distributions, we estimate three-year moving-average emissions of summertime NO_x from 35 US urban areas directly from NO_2 retrievals of the Ozone Monitoring Instrument (OMI) during 2005–2014. Following the conclusions of previous studies that the EMG method provides robust and accurate emission estimates under strong-wind conditions, we derive top-down NO_x emissions from each urban area by applying the EMG method to OMI data with wind speeds greater than $3\text{--}5\text{ m s}^{-1}$. Meanwhile, we find that OMI NO_2 observations under weak-wind conditions (i.e., $< 3\text{ m s}^{-1}$) are qualitatively better correlated with the surface NO_x source strength in comparison to all-wind OMI maps; and therefore we use them to calculate the satellite-observed NO_2 burdens of urban areas and compare with NO_x emission estimates. The EMG results show that OMI-derived NO_x emissions are highly correlated ($R > 0.93$) with weak-wind OMI NO_2 burdens as well as bottom-up NO_x emission estimates over 35 urban areas, implying a linear response of the OMI observations to surface emissions under weak-wind conditions. The simultaneous, EMG-obtained, effective NO_2 lifetimes ($\sim 3.5 \pm 1.3\text{ h}$), however, are biased low in comparison to the summertime NO_2 chemical lifetimes. In general, isolated urban areas with NO_x emission intensities greater than $\sim 2\text{ Mg h}^{-1}$ produce statistically significant weak-wind signals in three-year average OMI data. From 2005 to 2014, we estimate that total OMI-derived NO_x emissions over all selected US urban areas decreased by 49 %, consistent with reductions of 43, 47, 49, and 44 % in the total bottom-up NO_x emissions, the sum of weak-wind OMI NO_2 columns, the total weak-wind OMI NO_2 burdens, and the averaged NO_2 concentrations, respectively, reflecting the success of NO_x control programs for both mobile sources and power plants. The decrease rates of these NO_x -related quantities are found to be faster (i.e., -6.8 to $-9.3\% \text{ yr}^{-1}$) before 2010 and slower (i.e., -3.4 to $-4.9\% \text{ yr}^{-1}$) after

Estimation of US urban NO_x emissions from OMI

Z. Lu et al.

Title Page

Abstract

Introduction

Conclusions

References

Tables

Figures



Back

Close

Full Screen / Esc

Printer-friendly Version

Interactive Discussion



Estimation of US urban NO_x emissions from OMI

Z. Lu et al.

Title Page

Abstract

Introduction

Conclusions

References

Tables

Figures



Back

Close

Full Screen / Esc

Printer-friendly Version

Interactive Discussion



2010. For individual urban areas, we calculate the R values of pair-wise trends among the OMI-derived and bottom-up NO_x emissions, the weak-wind OMI NO₂ burdens, and ground-based NO₂ measurements; and high correlations are found for all urban areas (median $R = 0.8$), particularly large ones (R up to 0.97). The results of the current work indicate that using the EMG method and considering the wind effect, the OMI data allow for the estimation of NO_x emissions from urban areas and the direct constraint of emission trends with reasonable accuracy.

1 Introduction

Nitrogen oxides (NO_x), the sum of nitrogen dioxide (NO₂) and nitric oxide (NO), is one of the six criteria pollutants identified by the U.S. Environmental Protection Agency (EPA) under the requirement of the Clean Air Act. NO_x plays a crucial role in tropospheric chemistry processes such as the formation of ground-level ozone and secondary inorganic and organic aerosols; and thus it is also linked with other criteria pollutants including ozone, particulate matter, carbon monoxide, and sulfur oxides. Therefore, NO_x is not only harmful to human health, but also implicated in a number of environmental problems, such as acid rain, smog, eutrophication, climate change, etc. NO_x emissions come from both anthropogenic (e.g., man-made combustion of fossil fuels, biofuel, and biomass) and natural sources (e.g., lightning, microbial processes in soils, and wildfires). Bottom-up inventories of NO_x can be quite uncertain, because the emission factors of anthropogenic sources strongly depend on the fuel type, technology, and combustion condition, while natural sources are inherently difficult to quantify.

Due to the strong absorption of NO₂ molecules in the visible wavelength range of the spectrum, satellite instruments based on the principle of optical absorption spectroscopy serve as powerful tools to detect NO₂ signals from space at high temporal and spatial resolution (Martin, 2008 and references therein). The short lifetime of NO_x in the atmosphere leads to a close correlation between observed NO₂ columns and surface NO_x emission sources, implying the potential of space-borne instruments to aid in

**Estimation of US
urban NO_x emissions
from OMI**

Z. Lu et al.

Title Page

Abstract

Introduction

Conclusions

References

Tables

Figures



Back

Close

Full Screen / Esc

Printer-friendly Version

Interactive Discussion



the estimation of NO_x emissions (Streets et al., 2013, 2014; and references therein). In the past two decades, satellite remote sensing of tropospheric NO₂ columns has been widely and successfully used to map the spatial distributions of NO₂ at local, regional, and global scales (e.g., Kim et al., 2009; Russell et al., 2010; Boersma et al., 2007, 2011; Martin et al., 2003), identify intensive point and area NO_x emission sources (e.g., Duncan et al., 2013; Kim et al., 2006; Lu and Streets, 2012; Streets et al., 2014; Wang et al., 2010; Zhang et al., 2009), and monitor diurnal/weekly/monthly/interannual variations of NO₂ (e.g., Hilboll et al., 2013; Hudman et al., 2010; Richter et al., 2005; Russell et al., 2012; Schneider et al., 2015; Tong et al., 2015; van der A et al., 2008) for both anthropogenic and natural sources.

In general, local, regional, and global NO_x emissions can be verified, estimated, and optimized by using forward and inverse modeling of satellite NO₂ columns (e.g., Boersma et al., 2005; Jaeglé et al., 2005; Kim et al., 2009; Martin et al., 2003; Wang et al., 2012). However, NO_x emissions and NO₂ lifetimes can also be determined directly by analyzing the downwind patterns of the satellite-observed NO₂ columns near the sources. Leue et al. (2001) used an exponential function to fit the downwind decay of GOME (Global Ozone Monitoring Experiment)-observed NO₂ columns at the eastern shore of the US and estimated the NO₂ lifetime by using the fitted *e*-folding distance and the averaged wind velocity. Kunhikrishnan et al. (2004) conducted a similar analysis over the Arabian Sea outflow region to estimate the regional NO_x lifetime for the Indian subcontinent. This method was revised by Beirle et al. (2004), who fitted the GOME-observed NO₂ columns across the shipping lane between Sri Lanka and Indonesia with an exponentially-modified Gaussian (EMG) function and derived the mean NO_x lifetime and the corresponding ship emissions for 1996–2001. Hereinafter, we call this approach the EMG method. By fitting the downwind line densities of the OMI (Ozone Monitoring Instrument)-observed NO₂ separately for eight wind directions, Beirle et al. (2011) further improved the EMG method and determined the average NO_x emissions and lifetimes simultaneously for nine worldwide megacities during 2005–2009. Using a similar method, Ialongo et al. (2014) estimated the aver-

Estimation of US urban NO_x emissions from OMI

Z. Lu et al.

Title Page

Abstract

Introduction

Conclusions

References

Tables

Figures



Back

Close

Full Screen / Esc

Printer-friendly Version

Interactive Discussion



age summertime NO_x emissions and lifetimes of three cities in the Baltic Sea region during 2005–2011. The EMG method and its variant versions have also been applied to the satellite observations of SO₂ to constrain SO₂ lifetimes and emissions from volcanoes (Beirle et al., 2014; Krotkov et al., 2010; Theys et al., 2013; Carn et al., 2013) and large anthropogenic point sources (Fioletov et al., 2015).

Recently, several studies discussed the applicability and reliability of the EMG method. Valin et al. (2013) suggested that the NO_x emissions and chemical lifetimes would be better quantified when winds are fast because the downwind NO₂ decay under this condition is dominated by chemical removal, not variability of the winds. Introducing the plume rotation technique, they inferred NO_x emissions of Riyadh from the OMI measurements with fast winds (> 6.4 ms⁻¹) only and derived NO_x chemical lifetimes in slower wind conditions with the mass balance method. Additionally, de Foy et al. (2014) evaluated the performance of the EMG method using simulated column densities over a point source with known emissions under three chemical lifetime cases. They found that the EMG method generally provided reliable emission estimates at fast wind-speed conditions (> 3 ms⁻¹); however, the lifetime estimates were biased low and quite sensitive to the selection of the wind speed cut-off and the accuracy of the plume rotation. This implies that, in practice, the EMG-derived lifetimes should not be treated as chemical lifetimes, but rather as “effective lifetimes” that include the influences of chemical conversion, plume meandering, grid resolution, sampling issues, etc. (see also Fioletov et al., 2015; Ialongo et al., 2014). Nevertheless, the EMG method can provide quite accurate emission estimates if the issues of wind speed and direction are appropriately treated.

In this study, we use the OMI NO₂ retrievals and an EMG method to estimate NO_x emissions from 35 major US urban areas during the OMI era of 2005–2014. Although there have been a number of studies reporting satellite observations of NO₂ over some US cities, they mainly focused on the interannual trends and/or monthly/weekly variations of the satellite signals themselves (van der A et al., 2008; Hilboll et al., 2013; Schneider et al., 2015; Russell et al., 2012; Kim et al., 2009) or the comparison of satel-

served satellite NO₂ signals (Fig. 1a). We combined adjacent urban areas that share the same NO₂ hotspot (e.g., Washington, DC and Baltimore, Los Angeles and Riverside) and omitted some urban areas where the NO₂ signals are not isolated due to the influence of large NO_x emitting sources nearby (e.g., Pittsburgh, Milwaukee, San Francisco). In total, 35 urban areas were selected for analysis, and they together accounted for ~ 23 % of total NO_x emissions and ~ 50 % of total urban population in the US during the period 2005–2014.

2.3 Wind fields

Wind information (including speed and direction) is crucial in exploring its influence on the OMI NO₂ observations and estimating the NO_x emissions with the exponentially-modified Gaussian (EMG) method described in Sect. 2.4. In this work, we use the wind fields of ERA-interim reanalysis developed by the European Center for Medium-range Weather Forecast (ECMWF) (Dee et al., 2011). The ERA-interim reanalysis provides global wind fields of 60 vertical levels at four time steps per day (i.e., 0:00, 6:00, 12:00, 18:00 UTC) from 1979 to present on the N128 reduced Gaussian grid. Valin et al. (2013) expected that the EMG results would be insensitive to the choice of wind field datasets. This was confirmed by de Foy et al. (2015) who tested wind fields of both the ERA-interim reanalysis and the North American Regional Reanalysis (NARR) and obtained similar results in the EMG analysis. Furthermore, the ERA-interim reanalysis dataset has been proven to reproduce the observed spatial transport pattern of the OMI NO₂ successfully at the daily level (Beirle et al., 2011; Valin et al., 2013). The NO_x emitted near the surface of the urban areas can undergo rapid vertical mixing, and we thus used the averaged wind fields of the bottom eight levels (i.e., from surface to ~ 500 m), similar to the treatment of Beirle et al. (2011). We assume that the daily OMI NO₂ spatial pattern of a hotspot should not reflect the wind strength and direction at the OMI overpass time of ~ 13:45 LT, but the average wind fields in a few hours before the satellite takes the measurement. For simplicity, we chose 12:00 LT as the time of the wind fields. Consequently, daily wind speed and wind direction maps over

Estimation of US urban NO_x emissions from OMI

Z. Lu et al.

Title Page

Abstract

Introduction

Conclusions

References

Tables

Figures



Back

Close

Full Screen / Esc

Printer-friendly Version

Interactive Discussion



the entire domain of the US were interpolated temporally at 12:00 LT and spatially on a 2 km × 2 km grid in association with the oversampled OMI NO₂ maps.

2.4 Exponentially-modified Gaussian method

Beirle et al. (2011) presented a method using an EMG function to fit the downwind patterns of OMI NO₂ line densities separately for eight wind directions, and simultaneously determined the NO_x emissions and lifetimes of nine megacities around the world. In this work, we follow a similar methodology but with a number of enhancements. For each urban area, we did not separate the OMI NO₂ measurements into different wind directions, but rotated and overlapped the daily OMI NO₂ maps in the range of 300 km around the urban center (see Table 1 for the latitudes and the longitudes) to align all the wind directions at the urban center in the *x* direction (Valin et al., 2013; de Foy et al., 2014, 2015). This process increases the number of OMI samples, potentially increases the signal-to-noise ratio, and benefits the trend analysis using the EMG method. The wind-aligned OMI NO₂ maps were further reduced to one-dimension line densities by integrating the NO₂ data in the across-wind direction over a maximum interval of ±120 km (e.g., Chicago in Fig. 2). Depending on the size of the urban areas, smaller cross-wind integration intervals down to ±60 km were chosen for smaller NO₂ hotpots to minimize interference with the background NO₂ and the neighboring NO_x sources. The EMG model proposed by Beirle et al. (2011) was then used to fit the NO₂ line densities. As a function of the distance from the urban center *x*, the EMG model is expressed as Eqs. (1) to (3)

$$\text{OMI}_{\text{NO}_2, \text{line}}(x|\mu, \sigma, x_0, \alpha, B) = \alpha \cdot f(x|\mu, \sigma, x_0) + B = \alpha \cdot [e(x|x_0, \mu) \otimes G(x|\sigma)] + B \quad (1)$$

$$e(x|x_0, \mu) = \exp\left(-\frac{x-\mu}{x_0}\right) \quad \text{for } x \geq \mu, \text{ otherwise } e(x|x_0, \mu) = 0 \quad (2)$$

$$G(x|\sigma) = \frac{1}{\sqrt{2\pi}\sigma} \exp\left(-\frac{x^2}{2\sigma^2}\right) \quad (3)$$

Estimation of US urban NO_x emissions from OMI

Z. Lu et al.

Title Page	
Abstract	Introduction
Conclusions	References
Tables	Figures
◀	▶
◀	▶
Back	Close
Full Screen / Esc	
Printer-friendly Version	
Interactive Discussion	



The estimation problem is nonlinear with five parameters to be determined (i.e., μ , σ , x_0 , α , and B). Mathematically, Eqs. (1) to (3) can be written as (Kalambet et al., 2011 and references therein)

$$\text{OMI}_{\text{NO}_2, \text{line}}(x|\mu, \sigma, x_0, \alpha, B) = \alpha \cdot \left[\frac{1}{x_0} \exp\left(\frac{\mu}{x_0} + \frac{\sigma^2}{2x_0^2} - \frac{x}{x_0}\right) \Phi\left(\frac{x-\mu}{\sigma} - \frac{\sigma}{x_0}\right) \right] + B \quad (4)$$

5 where x_0 in the exponential function $e(x)$ is the e -folding distance downwind representing the length scale of the NO_2 decay; μ is the location of the apparent source relative to the city center; σ is the standard deviation of the Gaussian function $G(x)$, representing the Gaussian smoothing length scale; Φ is the cumulative distribution function; B is the offset factor representing the background NO_2 ; $f(x)$ is the convolution
 10 of $e(x)$ and $G(x)$; and α is the scale factor of $f(x)$. Since the integration of $f(x)$ equals one, the parameter α physically means the total number of NO_2 molecules observed near the hotspot, excluding the effect of the background NO_2 . α can be converted to mass units, representing the observed OMI NO_2 burden over the urban areas. Using the mean zonal wind speed w of the NO_2 line density domain, the mean effective
 15 NO_2 lifetime $\tau_{\text{effective}}$ and the mean NO_x emissions E can be calculated from the fitted parameter x_0 and α as

$$\tau_{\text{effective}} = x_0/w \quad (5)$$

$$E = 1.32 \cdot \alpha / \tau_{\text{effective}} = 1.32 \cdot \alpha \cdot w / x_0 \quad (6)$$

where the factor of 1.32 is the mean $\text{NO}_x / \text{NO}_2$ ratio suggested by Beirle et al. (2011).

20 We made additional treatments in processing the OMI NO_2 data and using the EMG method. For urban areas surrounded by significant NO_x emission sources, we discarded the OMI data with certain wind directions in the plume rotation process to limit the influence of surrounding sources on the wind-aligned OMI NO_2 line densities. For example, Washington, DC is located ~ 150 km southwest of Philadelphia. On the one

Estimation of US urban NOx emissions from OMI

Z. Lu et al.

Title Page	
Abstract	Introduction
Conclusions	References
Tables	Figures
◀	▶
◀	▶
Back	Close
Full Screen / Esc	
Printer-friendly Version	
Interactive Discussion	



**Estimation of US
urban NO_x emissions
from OMI**

Z. Lu et al.

Title Page

Abstract

Introduction

Conclusions

References

Tables

Figures



Back

Close

Full Screen / Esc

Printer-friendly Version

Interactive Discussion



The effect of different wind speeds on the patterns of the OMI-observed NO₂ columns was first shown by Valin et al. (2013) for Riyadh, Saudi Arabia. Here, we take Chicago as an example to demonstrate this effect. Figure 2a and b displays the wind-aligned OMI NO₂ TVCD maps of Chicago when wind speeds are slow ($< 3 \text{ ms}^{-1}$) and fast ($> 5 \text{ ms}^{-1}$), respectively. The corresponding NO₂ line densities are shown in Fig. 2c. At low wind speed NO_x emissions accumulate and stagnate near the urban center, making the peak NO₂ columns about twice those observed at high wind speed if the background NO₂ is removed. In contrast, NO₂ plumes can be transported further at the high wind speed condition, increasing the downwind NO₂ columns at 250 km from the urban center by $\sim 0.9 \times 10^{15} \text{ molecules cm}^{-2}$. These results clearly indicate that the presence of winds, especially high-speed winds, affects the satellite NO₂ observations.

In practice, OMI NO₂ TVCD maps are averaged from valid pixel data with winds at different speeds from different directions (e.g., Figs. 1a, 3a and b), and consequently, NO₂ signals near the NO_x emitting sources are smeared spatially. Figure 1b shows the summer mean NO₂ TVCDs over the US during 2005–2014 at wind speeds $< 3 \text{ ms}^{-1}$, and the maps for 2005–2007 and 2012–2014 are shown in Fig. 3d and e, respectively. Compared to NO₂ maps under the all-wind condition, NO₂ signals at low wind speeds are obviously higher over the urban areas (as well as in the big isolated power plant areas) and lower in surrounding rural areas (Figs. 1c, 3g and h), and consequently, more NO₂ hotspots are visible. In sum, satellite NO₂ maps for low wind-speed conditions highlight the NO_x emission sources. This is also demonstrated in a recent study by Ialongo et al. (2014), who used the OMI pixels with wind speeds $< 5 \text{ ms}^{-1}$ to highlight the NO_x signals of three cities over the Baltic Sea region.

The effect of winds on satellite-observed NO₂ columns is not uniform, but depends on the characteristics of the wind fields at each urban location. Figure 4 compares the OMI NO₂ TVCD maps for Chicago and Los Angeles under the all-wind and the weak-wind conditions. Compared to the significant differences in NO₂ columns over Chicago, the discrepancies between the weak-wind and the all-wind conditions over Los Angeles are nearly negligible. The reason is attributed to the different wind fields

Estimation of US urban NO_x emissions from OMI

Z. Lu et al.

Title Page

Abstract

Introduction

Conclusions

References

Tables

Figures



Back

Close

Full Screen / Esc

Printer-friendly Version

Interactive Discussion



average wind speed of at least 2 ms^{-1} was required for a target area to guarantee clear downwind outflow NO₂ patterns. However, Valin et al. (2013) pointed out that the variations of wind speed impact the nonlinear NO_x chemistry, and the NO₂ lifetime (and NO_x emissions) inferred from the average spatial pattern of the NO₂ plume is not necessarily equal to the average lifetime (and emissions). They restricted their analysis to OMI measurements made when winds were fast (i.e., $> 6.4 \text{ ms}^{-1}$) because under this condition the downwind decay of NO₂ is dominated by chemical removal, not variability of the winds. Recently, de Foy et al. (2014) evaluated the EMG method using simulated column densities over an ideal point source with different chemical lifetimes and wind speeds. They found that the EMG method provided fairly robust and accurate emission estimates when wind speeds were larger than 3 ms^{-1} . In this work, we therefore apply the EMG method to the OMI line densities under strong wind-speed conditions to estimate NO_x emissions. The criterion for the wind speed was set to be above 5 ms^{-1} and, if necessary, relaxed to 4 or 3 ms^{-1} to ensure at least 30 valid OMI samples in three consecutive years.

Again, we use the example of Chicago to demonstrate our analytical procedure. Figure 2b shows the wind-aligned OMI NO₂ TVCDs at wind speeds $> 5 \text{ ms}^{-1}$ for Chicago during 2005–2007 (i.e., the year 2006*). The NO₂ line densities and the corresponding EMG fit are shown in Fig. 2c. Clearly, the EMG fit reproduces the NO₂ pattern along the wind direction very well. The fitted e -folding distance x_0 , background B , and the burden α are 144 km, $9.83 \times 10^3 \text{ mol km}^{-1}$, and $2.74 \times 10^6 \text{ mol}$, respectively. The average wind speed w of valid OMI pixels over the studied domain is 7.3 ms^{-1} , so that the effective NO₂ lifetime $\tau_{\text{effective}}$ and the NO_x emissions E are determined to be 5.5 h and 30 Mg h^{-1} through Eqs. (5) and (6), respectively. We also use the EMG method to fit the NO₂ line densities at wind speeds $< 3 \text{ ms}^{-1}$ (see Fig. 2 and Sect. 3.1), and the OMI NO₂ burden under the weak-wind condition is estimated to be 98 Mg. The same analysis is conducted for all the three-consecutive-years during 2005–2014 and the three-year moving NO₂ and NO_x trends are summarized in Fig. 5. Results show that the four NO_x-related trends in Chicago correlate with each other very well from

Estimation of US urban NO_x emissions from OMI

Z. Lu et al.

Title Page

Abstract

Introduction

Conclusions

References

Tables

Figures



Back

Close

Full Screen / Esc

Printer-friendly Version

Interactive Discussion



sidered as a combination of τ_{chemical} and an extra lifetime term of τ_{extra} related to the influences of plume meandering, grid resolution, and sampling issues (i.e., lifetimes are combined inversely as shown in Eq. 7) (de Foy et al., 2014, 2015). As summarized in Table 1, the estimated $\tau_{\text{effective}}$ were in the range of 1.2–6.8 h with a mean of $\sim 3.5 \pm 1.3$ h for all studied urban areas during 2005–2014. They are biased low in comparison to the expected summertime NO₂ τ_{chemical} of ~ 7 h estimated for a broader region in the Eastern United States (Lamsal et al., 2010) confirming the findings by de Foy et al. (2014), but are consistent with previously reported summertime NO₂ lifetimes of 1–7 h examined over plumes of urban areas (Beirle et al., 2011; Dommen et al., 1999; Ialongo et al., 2014; Nunnermacker et al., 1998; Spicer, 1982), power plants (Fioletov et al., 2015; Nunnermacker et al., 2000; Sillman, 2000), and open biomass burning (Alvarado et al., 2010; Mebust et al., 2011).

It should be noted that the slopes of the regression lines of ~ 2.8 h in Fig. 6a and b are also a time term. It can be considered as an average time scale of the OMI-observed NO₂ residency over the emission sources under the slow wind condition. We therefore name it the residence lifetime $\tau_{\text{residence}}$ as suggested by de Foy et al. (2014). In addition to $\tau_{\text{effective}}$, $\tau_{\text{residence}}$ includes the influences of NO₂ physical dispersion in the atmosphere, and can be calculated approximately as

$$\frac{1}{\tau_{\text{residence}}} = \frac{1}{\tau_{\text{dispersion}}} + \frac{1}{\tau_{\text{effective}}} = \frac{1}{\tau_{\text{dispersion}}} + \frac{1}{\tau_{\text{chemical}}} + \frac{1}{\tau_{\text{extra}}} \quad (7)$$

where $\tau_{\text{dispersion}}$ is the physical dispersion time scale. For the slow wind speeds condition, the average fitting interval downwind from the urban center was 150 km and the average wind speed was 2 m s^{-1} . Hence, $\tau_{\text{dispersion}}$ was about 21 h and the average $\tau_{\text{residence}}$ for all the urban areas was estimated to be ~ 3 h using Eq. (7), assuming that $\tau_{\text{effective}}$ did not change significantly with wind speed. This $\tau_{\text{residence}}$ estimation is close to the ones derived directly from Fig. 6a and b (i.e., 2.8 h).

Figure 6c shows the comparison between the OMI-derived and the NEI NO_x emissions for all the selected urban areas. Good agreement was also found between the

Estimation of US urban NO_x emissions from OMI

Z. Lu et al.

Title Page

Abstract

Introduction

Conclusions

References

Tables

Figures



Back

Close

Full Screen / Esc

Printer-friendly Version

Interactive Discussion



only six areas have an average correlation coefficient < 0.7 . The NO_x-related trends are in better agreement with each other for the larger OMI NO₂ hotspots such as New York, Los Angeles, Chicago, Philadelphia, and Washington, DC (mean $R > 0.92$). The poorest correlation among the four NO_x-related series is observed in New Orleans (mean $R = 0.48$), where NO_x emissions are close to the lowest detection limit of the EMG method we suggested in Sect. 3.2 ($\sim 2 \text{ Mg h}^{-1}$).

The differences in trends of the four NO_x-related quantities in individual urban areas can be attributed to the following reasons. For the OMI-derived NO₂ and NO_x emissions, we have discussed previously that the selection of the wind speed group and inaccuracy in the wind rotation affects the observed NO₂ trends and the EMG fitted results. Moreover, the EMG method is best suited to point sources; however, urban NO_x emissions are area sources, and the size and shape of the urban area may introduce additional uncertainty to the EMG results. For the NEI emissions, though NO_x emissions from power plants are measured directly using the continuous emissions monitoring system (CEMS), emissions from other sources (e.g., mobile emissions) are still estimated using bottom-up approaches, which have significant uncertainties inherent in the emission factors and the emissions models that are used (USEPA, 1996). For the AQS data, NO₂ measurements at a limited number of monitoring sites can be readily influenced by nearby emission sources and thus may sometimes reflect localized trends rather than urban-scale trends (e.g., Lamsal et al., 2015). Last but not least, there are spatial and temporal mismatches among emissions, OMI observations, and AQS data (e.g., Tong et al., 2015; Bechle et al., 2013). Spatially, OMI provides measurements of tropospheric NO₂ column densities; AQS data are nose-level NO₂ concentrations; while emissions are NO_x masses directly discharged into the atmosphere at a variety of heights above the surface. Temporally, the NEI emissions are annual estimates; the OMI data were restricted to the summer half-year and have gone through a series of filtering processes to remove unreliable pixels; and, although we restricted our analysis to the hourly NO₂ measurements close to the OMI overpass time, all AQS measurements at the chosen sites in April–September were used for the trend comparison.

Estimation of US urban NO_x emissions from OMI

Z. Lu et al.

Title Page

Abstract

Introduction

Conclusions

References

Tables

Figures



Back

Close

Full Screen / Esc

Printer-friendly Version

Interactive Discussion



size chosen for each area, trend calculation method used, etc., they derived similar average NO₂ column decrease rates of -5.8 to $-6.2\% \text{ yr}^{-1}$ for US cities since ~ 2005 . This implies that the differences mentioned above may have minor influence on the overall trend analysis results at the country or regional level. However, we obtain a significantly greater column decrease rate of $-7.3\% \text{ yr}^{-1}$ in this work. As discussed in Sect. 3.1, the fact that all these previous studies used all-wind satellite NO₂ maps while we used weak-wind OMI data is the major reason for such discrepancy.

In previous studies such as Russell et al. (2012), Tong et al. (2015), and Lamsal et al. (2015), OMI NO₂ reduction rates were observed to be moderate ($\sim -7\% \text{ yr}^{-1}$), larger ($\sim -9\% \text{ yr}^{-1}$), and smaller ($\sim -3\% \text{ yr}^{-1}$) during the periods of 2005–2007, 2008–2009, and after 2010, respectively, over the US urban areas. The reason for these changes of pace of the reduction was attributed in these previous studies to the combined effects of the gradually installed NO_x control devices in power plants, transformation to a less-polluting vehicle fleet, the economic recession that happened in 2008, and the slow recovery of the US economy after 2008. In this work, we found similar trends. As shown in Figs. 8 and 9, the sum of OMI columns, the total NEI NO_x emissions, OMI-derived NO_x emissions, OMI NO₂ burdens, and the average NO₂ concentrations over selected urban areas decreased at rates of -6.8 to $-9.3\% \text{ yr}^{-1}$ during 2006*–2010*, and -3.4 to $-4.6\% \text{ yr}^{-1}$ during 2010*–2013* (Table 2). We did not observe a greater decreasing rate during the economic recession period, probably because we used three-year moving trends which smooth the short-term changes. Extrapolating the trends to the years of 2005 and 2014 with AADRs of earlier and later periods, respectively, we estimate that the above five NO_x-related quantities decreased by approximately 47, 43, 49, 49, and 44 %, respectively, during the whole period of 2005–2014.

Although satellite NO₂ column changes cannot be translated to NO_x emission changes directly, due to the nonlinear feedback of NO_x emissions on NO_x chemistry (Lamsal et al., 2011; Lu and Streets, 2012), we indeed obtained similar reductions in total NO_x emissions and total OMI NO₂ observations over all the selected urban ar-

eas in the US. Lamsal et al. (2011) used a dimensionless factor of β to express the relationship between changes in NO_x emissions and changes in NO_2 TVCDs:

$$\beta = \frac{\Delta E/E}{\Delta \text{TVCD}/\text{TVCD}} \quad (8)$$

Generally, β is greater than one in clean regions, because increased NO_x emissions under the low NO_2 condition promotes the generation of OH radicals and thus decreases the NO_x lifetime, while β is less than one in polluted regions since an increase in NO_x emissions consumes OH radicals and increases the NO_x lifetime. On the basis of the monthly global gridded β calculated by Lamsal et al. (2011), the average β over the 35 selected urban areas during April–September was 1.03 ± 0.21 (bounding values 0.74–1.52). That partially explains why we observed similar trends in total NO_x emissions and total OMI NO_2 columns in this work. It should be noted that we only discuss the overall atmospheric characteristics over all urban areas here. Individual areas may have β values significantly greater or smaller than one reflecting the local sensitivity of changes in OMI NO_2 columns to NO_x emissions.

4 Summary and conclusions

In the present work, we use the satellite observations of NO_2 vertical columns from the OMI instrument to quantify the summer half-year (i.e., April–September) NO_x emissions and emission trends of 35 selected US urban areas during 2005–2014. To refine the analysis, we first explore the impact of winds on the satellite NO_2 observations. Significant differences are found between the OMI NO_2 maps averaged from all valid data and those from data with slow wind speeds only, and such differences are not uniform across all urban areas but depend on local meteorological conditions. Compared to NO_2 maps under all-wind conditions, the satellite-observed NO_2 signals at wind speeds $< 3 \text{ m s}^{-1}$ are significantly higher over the urban areas and lower in surrounding rural areas, and are better correlated to the amounts of surface NO_x emissions. We

Estimation of US urban NO_x emissions from OMI

Z. Lu et al.

Title Page

Abstract

Introduction

Conclusions

References

Tables

Figures



Back

Close

Full Screen / Esc

Printer-friendly Version

Interactive Discussion



observe greater NO₂ column reductions over a number of selected cities from 2006* (i.e., 2005–2007) to 2013* (i.e., 2012–2014) under the weak-wind condition than under the all-wind condition, implying that the effect of winds should be taken into account when comparing the trends of NO_x emissions and satellite NO₂ observations.

Noticing the importance of wind speed, we divide the OMI observations around each urban area into fast (> 3 to 5 m s⁻¹) and slow (< 3 m s⁻¹) wind-speed groups. Daily OMI NO₂ data of each wind-speed group are rotated and oversampled to generate wind-aligned OMI NO₂ maps, the along-wind line densities of which are further fitted by an exponentially-modified Gaussian (EMG) function. For each urban area in any three consecutive years during 2005–2014, we derive the corresponding NO_x emissions and effective NO₂ lifetimes from the EMG fits of the fast wind-speed groups and the OMI NO₂ burdens from the slow wind-speed groups. We find good linear agreement ($R > 0.93$) among NEI NO_x emissions, OMI-derived NO_x emissions, and OMI NO₂ burdens, implying the possibility of using the satellite NO₂ observations under the weak-wind condition to constrain the surface NO_x emissions directly. The simultaneously obtained effective NO₂ lifetimes ($\sim 3.5 \pm 1.3$ h) are biased low in comparison to the summertime NO₂ chemical lifetime of ~ 7 h, reflecting the influences of plume meandering and the coarse sampling resolution on the EMG fitted results.

Finally, we quantify the NO_x reductions in selected US urban areas and compare the trends of satellite observations with those of bottom-up emissions and ground-based measurements. We find that the time series of the NO_x-related quantities correlate with each other very well in most US urban areas, especially for large cities. Due to the successful control of NO_x emissions in both the power and transportation sectors, the total NEI NO_x emissions, the total OMI-derived NO_x emissions, the sum of OMI NO₂ columns (under the weak winds condition), the total OMI NO₂ burdens (under the weak winds condition), and the average measured NO₂ concentrations for all US urban areas decreased by 43, 49, 47, 49, and 44 %, respectively, from 2005 to 2014. Reductions of these five NO_x-related quantities were rapid, at rates of -6.8 to -9.3 % yr⁻¹, before 2010 and slowed down to rates of -3.4 to -4.9 % yr⁻¹ in recent years. Generally, the

Estimation of US urban NO_x emissions from OMI

Z. Lu et al.

[Title Page](#)[Abstract](#)[Introduction](#)[Conclusions](#)[References](#)[Tables](#)[Figures](#)[Back](#)[Close](#)[Full Screen / Esc](#)[Printer-friendly Version](#)[Interactive Discussion](#)

annual average rates of decrease of OMI NO₂ observations obtained in this work are greater than previously reported values derived from the all-wind satellite maps, further demonstrating the importance of considering winds.

We have shown that using the EMG method, the OMI has the capability to estimate NO_x emissions from urban areas directly and constrain their trends with reasonable accuracy. These OMI-derived emissions can provide independent and valuable information to policy makers and researchers in verifying the bottom-up emission estimates and inspecting the effectiveness of emission control measures, especially for areas without complete surface monitoring networks and lacking well-established emission inventories. We also show that a comprehensive and integrated analysis of satellite observations, ground measurements, and bottom-up emissions can overcome shortcomings of the individual datasets and provide a better understanding of the true NO_x situation in a given area. Furthermore, the method described in this work can be applied to the near-future satellite missions such as NASA's Tropospheric Emissions: Monitoring of Pollution (TEMPO, Chance et al., 2013) and the European Space Agency's (ESA) Tropospheric Ozone Monitoring Instrument (TROPOMI, Veefkind et al., 2012). With the improved temporal and/or spatial resolution offered by these missions, the diurnal variations of NO_x emissions and emissions from smaller sources are likely to be able to be inferred.

The Supplement related to this article is available online at doi:10.5194/acpd-15-14961-2015-supplement.

Acknowledgements. This work was sponsored by the National Aeronautics and Space Administration (NASA) as a part of the Air Quality Applied Sciences Team (AQAST) program, for which we are grateful to the NASA Project Officer John Haynes and the AQAST team leader Daniel Jacob. We acknowledge the free use of tropospheric NO₂ column data from the OMI sensor from www.temis.nl. Argonne National Laboratory is operated by UChicago Argonne, LLC, under Contract No. DE-AC02-06CH11357 with the U.S. Department of Energy.

Estimation of US urban NO_x emissions from OMI

Z. Lu et al.

Title Page

Abstract Introduction

Conclusions References

Tables Figures

◀ ▶

◀ ▶

Back Close

Full Screen / Esc

Printer-friendly Version

Interactive Discussion



References

- Alvarado, M. J., Logan, J. A., Mao, J., Apel, E., Riemer, D., Blake, D., Cohen, R. C., Min, K.-E., Perring, A. E., Browne, E. C., Wooldridge, P. J., Diskin, G. S., Sachse, G. W., Fuelberg, H., Sessions, W. R., Harrigan, D. L., Huey, G., Liao, J., Case-Hanks, A., Jimenez, J. L., Cubison, M. J., Vay, S. A., Weinheimer, A. J., Knapp, D. J., Montzka, D. D., Flocke, F. M., Pollock, I. B., Wennberg, P. O., Kurten, A., Crounse, J., Clair, J. M. St., Wisthaler, A., Mikoviny, T., Yantosca, R. M., Carouge, C. C., and Le Sager, P.: Nitrogen oxides and PAN in plumes from boreal fires during ARCTAS-B and their impact on ozone: an integrated analysis of aircraft and satellite observations, *Atmos. Chem. Phys.*, 10, 9739–9760, doi:10.5194/acp-10-9739-2010, 2010.
- Bechle, M. J., Millet, D. B., and Marshall, J. D.: Remote sensing of exposure to NO₂: satellite versus ground-based measurement in a large urban, *Atmos. Environ.*, 69, 345–353, 2013.
- Beirle, S., Platt, U., von Glasow, R., Wenig, M., and Wagner, T.: Estimate of nitrogen oxide emissions from shipping by satellite remote sensing, *Geophys. Res. Lett.*, 31, L18102, doi:10.1029/2004gl020312, 2004.
- Beirle, S., Boersma, K. F., Platt, U., Lawrence, M. G., and Wagner, T.: Megacity emissions and lifetimes of nitrogen oxides probed from space, *Science*, 333, 1737–1739, 2011.
- Beirle, S., Hörmann, C., Penning de Vries, M., Dörner, S., Kern, C., and Wagner, T.: Estimating the volcanic emission rate and atmospheric lifetime of SO₂ from space: a case study for Kīlauea volcano, Hawai‘i, *Atmos. Chem. Phys.*, 14, 8309–8322, doi:10.5194/acp-14-8309-2014, 2014.
- Boersma, K. F., Eskes, H. J., Meijer, E. W., and Kelder, H. M.: Estimates of lightning NO_x production from GOME satellite observations, *Atmos. Chem. Phys.*, 5, 2311–2331, doi:10.5194/acp-5-2311-2005, 2005.
- Boersma, K. F., Eskes, H. J., Veefkind, J. P., Brinksma, E. J., van der A, R. J., Sneep, M., van den Oord, G. H. J., Levelt, P. F., Stammes, P., Gleason, J. F., and Bucsela, E. J.: Near-real time retrieval of tropospheric NO₂ from OMI, *Atmos. Chem. Phys.*, 7, 2103–2118, doi:10.5194/acp-7-2103-2007, 2007.
- Boersma, K. F., Eskes, H. J., Dirksen, R. J., van der A, R. J., Veefkind, J. P., Stammes, P., Huijnen, V., Kleipool, Q. L., Sneep, M., Claas, J., Leitão, J., Richter, A., Zhou, Y., and Brunner, D.: An improved tropospheric NO₂ column retrieval algorithm for the Ozone Monitoring Instrument, *Atmos. Meas. Tech.*, 4, 1905–1928, doi:10.5194/amt-4-1905-2011, 2011.

Estimation of US urban NO_x emissions from OMI

Z. Lu et al.

Title Page

Abstract

Introduction

Conclusions

References

Tables

Figures



Back

Close

Full Screen / Esc

Printer-friendly Version

Interactive Discussion



Estimation of US urban NO_x emissions from OMI

Z. Lu et al.

[Title Page](#)
[Abstract](#)
[Introduction](#)
[Conclusions](#)
[References](#)
[Tables](#)
[Figures](#)

[Back](#)
[Close](#)
[Full Screen / Esc](#)
[Printer-friendly Version](#)
[Interactive Discussion](#)


- Carn, S. A., Krotkov, N. A., Yang, K., and Krueger, A. J.: Measuring global volcanic degassing with the Ozone Monitoring Instrument (OMI), in: *Remote Sensing of Volcanoes and Volcanic Processes: Integrating Observation and Modeling*, edited by: Pyle, D. M., Mather, T. A., and Biggs, J., Geological Society, Special Publications, 380, London, 229–257, 2013.
- 5 Chance, K., Liu, X., Suleiman, R. M., Flittner, D. E., Al-Saadi, J., and Janz, S. J.: Tropospheric emissions: monitoring of pollution (TEMPO), in: *Proc. SPIE 8866, Earth Observing Systems XVIII*, San Diego, California, USA, 25 August 2013, doi:10.1117/12.2024479, 2013.
- Dallmann, T. R. and Harley, R. A.: Evaluation of mobile source emission trends in the United States, *J. Geophys. Res.*, 115, D14305, doi:10.1029/2010jd013862, 2010.
- 10 de Foy, B., Krotkov, N. A., Bei, N., Herndon, S. C., Huey, L. G., Martínez, A.-P., Ruiz-Suárez, L. G., Wood, E. C., Zavala, M., and Molina, L. T.: Hit from both sides: tracking industrial and volcanic plumes in Mexico City with surface measurements and OMI SO₂ retrievals during the MILAGRO field campaign, *Atmos. Chem. Phys.*, 9, 9599–9617, doi:10.5194/acp-9-9599-2009, 2009.
- 15 de Foy, B., Wilkins, J. L., Lu, Z., Streets, D. G., and Duncan, B. N.: Model evaluation of methods for estimating surface emissions and chemical lifetimes from satellite data, *Atmos. Environ.*, 98, 66–77, 2014.
- de Foy, B., Lu, Z., Streets, D. G., Lamsal, L. N., and Duncan, B. N.: Obtaining accurate estimates of power plant NO_x emissions from satellite data, *Atmos. Environ.*, accepted, 2015.
- 20 Dee, D. P., Uppala, S. M., Simmons, A. J., Berrisford, P., Poli, P., Kobayashi, S., Andrae, U., Balmaseda, M. A., Balsamo, G., Bauer, P., Bechtold, P., Beljaars, A. C. M., van de Berg, L., Bidlot, J., Bormann, N., Delsol, C., Dragani, R., Fuentes, M., Geer, A. J., Haimberger, L., Healy, S. B., Hersbach, H., Holm, E. V., Isaksen, I., Kallberg, P., Kohler, M., Matricardi, M., McNally, A. P., Monge-Sanz, B. M., Morcrette, J. J., Park, B. K., Peubey, C., de Rosnay, P., Tavolato, C., Thepaut, J. N., and Vitart, F.: The ERA-Interim reanalysis: configuration and performance of the data assimilation system, *Q. J. Roy. Meteor. Soc.*, 137, 553–597, 2011.
- 25 Demerjian, K. L.: A review of national monitoring networks in North America, *Atmos. Environ.*, 34, 1861–1884, 2000.
- Dommen, J., Prevot, A. S. H., Hering, A. M., Staffelbach, T., Kok, G. L., and Schillawski, R. D.: Photochemical production and aging of an urban air mass, *J. Geophys. Res.*, 104, 5493–5506, 1999.
- 30 Duncan, B. N., Yoshida, Y., de Foy, B., Lamsal, L. N., Streets, D. G., Lu, Z., Pickering, K. E., and Krotkov, N. A.: The observed response of Ozone Monitoring Instrument (OMI) NO₂ columns

Estimation of US urban NO_x emissions from OMI

Z. Lu et al.

[Title Page](#)
[Abstract](#)
[Introduction](#)
[Conclusions](#)
[References](#)
[Tables](#)
[Figures](#)




[Back](#)
[Close](#)
[Full Screen / Esc](#)
[Printer-friendly Version](#)
[Interactive Discussion](#)


to NO_x emission controls on power plants in the United States: 2005–2011, *Atmos. Environ.*, 47, 102–111, 2013.

Fioletov, V. E., McLinden, C. A., Krotkov, N., Moran, M. D., and Yang, K.: Estimation of SO₂ emissions using OMI retrievals, *Geophys. Res. Lett.*, 38, L21811, doi:10.1029/2011gl049402, 2011.

Fioletov, V. E., McLinden, C. A., Krotkov, N., Yang, K., Loyola, D. G., Valks, P., Theys, N., Van Roozendaal, M., Nowlan, C. R., Chance, K., Liu, X., Lee, C., and Martin, R. V.: Application of OMI, SCIAMACHY, and GOME-2 satellite SO₂ retrievals for detection of large emission sources, *J. Geophys. Res.*, 118, 11399–11418, 2013.

Fioletov, V. E., McLinden, C. A., Krotkov, N., and Li, C.: Lifetimes and emissions of SO₂ from point sources estimated from OMI, *Geophys. Res. Lett.*, 42, 1969–1976, doi:10.1002/2015GL063148, 2015.

Hilboll, A., Richter, A., and Burrows, J. P.: Long-term changes of tropospheric NO₂ over megacities derived from multiple satellite instruments, *Atmos. Chem. Phys.*, 13, 4145–4169, doi:10.5194/acp-13-4145-2013, 2013.

Hudman, R. C., Russell, A. R., Valin, L. C., and Cohen, R. C.: Interannual variability in soil nitric oxide emissions over the United States as viewed from space, *Atmos. Chem. Phys.*, 10, 9943–9952, doi:10.5194/acp-10-9943-2010, 2010.

Ialongo, I., Hakkarainen, J., Hyttinen, N., Jalkanen, J.-P., Johansson, L., Boersma, K. F., Krotkov, N., and Tamminen, J.: Characterization of OMI tropospheric NO₂ over the Baltic Sea region, *Atmos. Chem. Phys.*, 14, 7795–7805, doi:10.5194/acp-14-7795-2014, 2014.

Jaeglé, L., Steinberger, L., Martin, R. V., and Chance, K.: Global partitioning of NO_x sources using satellite observations: relative roles of fossil fuel combustion, biomass burning and soil emissions, *Faraday Discuss.*, 130, 407–423, 2005.

Kalambet, Y., Kozmin, Y., Mikhailova, K., Nagaev, I., and Tikhonov, P.: Reconstruction of chromatographic peaks using the exponentially modified Gaussian function, *J. Chemometr.*, 25, 352–356, 2011.

Kim, S. W., Heckel, A., McKeen, S. A., Frost, G. J., Hsie, E. Y., Trainer, M. K., Richter, A., Burrows, J. P., Peckham, S. E., and Grell, G. A.: Satellite-observed US power plant NO_x emission reductions and their impact on air quality, *Geophys. Res. Lett.*, 33, L22812, doi:10.1029/2006gl027749, 2006.

Kim, S. W., Heckel, A., Frost, G. J., Richter, A., Gleason, J., Burrows, J. P., McKeen, S., Hsie, E. Y., Granier, C., and Trainer, M.: NO₂ columns in the western United States ob-

**Estimation of US
urban NO_x emissions
from OMI**

Z. Lu et al.

Title Page

Abstract

Introduction

Conclusions

References

Tables

Figures



Back

Close

Full Screen / Esc

Printer-friendly Version

Interactive Discussion



served from space and simulated by a regional chemistry model and their implications for NO_x emissions, *J. Geophys. Res.*, 114, D11301, doi:10.1029/2008jd011343, 2009.

Krotkov, N. A., Schoeberl, M. R., Morris, G. A., Carn, S., and Yang, K.: Dispersion and lifetime of the SO₂ cloud from the August 2008 Kasatochi eruption, *J. Geophys. Res.*, 115, D00120, doi:10.1029/2010jd013984, 2010.

Kunhikrishnan, T., Lawrence, M. G., von Kuhlmann, R., Richter, A., Ladstatter-Weissenmayer, A., and Burrows, J. P.: Analysis of tropospheric NO_x over Asia using the model of atmospheric transport and chemistry (MATCH-MPIC) and GOME-satellite observations, *Atmos. Environ.*, 38, 581–596, 2004.

Lamsal, L. N., Martin, R. V., van Donkelaar, A., Celarier, E. A., Bucsela, E. J., Boersma, K. F., Dirksen, R., Luo, C., and Wang, Y.: Indirect validation of tropospheric nitrogen dioxide retrieved from the OMI satellite instrument: insight into the seasonal variation of nitrogen oxides at northern midlatitudes, *J. Geophys. Res.*, 115, D05302, doi:10.1029/2009jd013351, 2010.

Lamsal, L. N., Martin, R. V., Padmanabhan, A., van Donkelaar, A., Zhang, Q., Sioris, C. E., Chance, K., Kurosu, T. P., and Newchurch, M. J.: Application of satellite observations for timely updates to global anthropogenic NO_x emission inventories, *Geophys. Res. Lett.*, 38, L05810, doi:10.1029/2010gl046476, 2011.

Lamsal, L. N., Duncan, B. N., Yoshida, Y., Krotkov, N. A., Pickering, K. E., Streets, D. G., and Lu, Z.: US NO₂ trends (2005–2013): EPA Air Quality System (AQS) data versus improved observations from the Ozone Monitoring Instrument (OMI), *Atmos. Environ.*, 110, 130–143, 2015.

Leue, C., Wenig, M., Wagner, T., Klimm, O., Platt, U., and Jahne, B.: Quantitative analysis of NO_x emissions from Global Ozone Monitoring Experiment satellite image sequences, *J. Geophys. Res.*, 106, 5493–5505, 2001.

Levelt, P. F., Van den Oord, G. H. J., Dobber, M. R., Malkki, A., Visser, H., de Vries, J., Stammes, P., Lundell, J. O. V., and Saari, H.: The Ozone Monitoring Instrument, *IEEE T. Geosci. Remote*, 44, 1093–1101, 2006.

Lu, Z. and Streets, D. G.: Increase in NO_x emissions from Indian thermal power plants during 1996–2010: unit-based inventories and multisatellite observations, *Environ. Sci. Technol.*, 46, 7463–7470, 2012.

Estimation of US urban NO_x emissions from OMI

Z. Lu et al.

[Title Page](#)
[Abstract](#)
[Introduction](#)
[Conclusions](#)
[References](#)
[Tables](#)
[Figures](#)




[Back](#)
[Close](#)
[Full Screen / Esc](#)
[Printer-friendly Version](#)
[Interactive Discussion](#)


Lu, Z., Streets, D. G., de Foy, B., and Krotkov, N. A.: Ozone Monitoring Instrument observations of interannual increases in SO₂ emissions from Indian coal-fired power plants during 2005–2012, *Environ. Sci. Technol.*, 47, 13993–14000, 2013.

Martin, R. V.: Satellite remote sensing of surface air quality, *Atmos. Environ.*, 42, 7823–7843, 2008.

Martin, R. V., Jacob, D. J., Chance, K., Kurosu, T. P., Palmer, P. I., and Evans, M. J.: Global inventory of nitrogen oxide emissions constrained by space-based observations of NO₂ columns, *J. Geophys. Res.*, 108, 4537, doi:10.1029/2003jd003453, 2003.

McDonald, B. C., Dallmann, T. R., Martin, E. W., and Harley, R. A.: Long-term trends in nitrogen oxide emissions from motor vehicles at national, state, and air basin scales, *J. Geophys. Res.*, 117, D00v18, doi:10.1029/2012jd018304, 2012.

Mebust, A. K., Russell, A. R., Hudman, R. C., Valin, L. C., and Cohen, R. C.: Characterization of wildfire NO_x emissions using MODIS fire radiative power and OMI tropospheric NO₂ columns, *Atmos. Chem. Phys.*, 11, 5839–5851, doi:10.5194/acp-11-5839-2011, 2011.

Nunnermacker, L. J., Imre, D., Daum, P. H., Kleinman, L., Lee, Y. N., Lee, J. H., Springston, S. R., Newman, L., Weinstein-Lloyd, J., Luke, W. T., Banta, R., Alvarez, R., Senff, C., Sillman, S., Holdren, M., Keigley, G. W., and Zhou, X.: Characterization of the Nashville urban plume on 3 July and 18 July 1995, *J. Geophys. Res.*, 103, 28129–28148, 1998.

Nunnermacker, L. J., Kleinman, L. I., Imre, D., Daum, P. H., Lee, Y. N., Lee, J. H., Springston, S. R., Newman, L., and Gillani, N.: NO_y lifetimes and O₃ production efficiencies in urban and power plant plumes: analysis of field data, *J. Geophys. Res.*, 105, 9165–9176, 2000.

Richter, A., Burrows, J. P., Nuss, H., Granier, C., and Niemeier, U.: Increase in tropospheric nitrogen dioxide over China observed from space, *Nature*, 437, 129–132, 2005.

Russell, A. R., Valin, L. C., Bucsela, E. J., Wenig, M. O., and Cohen, R. C.: Space-based constraints on spatial and temporal patterns of NO_x emissions in California, 2005–2008, *Environ. Sci. Technol.*, 44, 3608–3615, 2010.

Russell, A. R., Valin, L. C., and Cohen, R. C.: Trends in OMI NO₂ observations over the United States: effects of emission control technology and the economic recession, *Atmos. Chem. Phys.*, 12, 12197–12209, doi:10.5194/acp-12-12197-2012, 2012.

**Estimation of US
urban NO_x emissions
from OMI**

Z. Lu et al.

[Title Page](#)[Abstract](#)[Introduction](#)[Conclusions](#)[References](#)[Tables](#)[Figures](#)[Back](#)[Close](#)[Full Screen / Esc](#)[Printer-friendly Version](#)[Interactive Discussion](#)

Schneider, P., Lahoz, W. A., and van der A, R.: Recent satellite-based trends of tropospheric nitrogen dioxide over large urban agglomerations worldwide, *Atmos. Chem. Phys.*, 15, 1205–1220, doi:10.5194/acp-15-1205-2015, 2015.

Sillman, S.: Ozone production efficiency and loss of NO_x in power plant plumes: photochemical model and interpretation of measurements in Tennessee, *J. Geophys. Res.*, 105, 9189–9202, 2000.

Spicer, C. W.: Nitrogen-oxide reactions in the urban plume of Boston, *Science*, 215, 1095–1097, 1982.

Streets, D. G., Canty, T., Carmichael, G. R., de Foy, B., Dickerson, R. R., Duncan, B. N., Edwards, D. P., Haynes, J. A., Henze, D. K., Houyoux, M. R., Jacob, D. J., Krotkov, N. A., Lamsal, L. N., Liu, Y., Lu, Z., Martini, R. V., Pfister, G. G., Pinder, R. W., Salawitch, R. J., and Wechti, K. J.: Emissions estimation from satellite retrievals: a review of current capability, *Atmos. Environ.*, 77, 1011–1042, 2013.

Streets, D. G., de Foy, B., Duncan, B. N., Lamsal, L. N., Li, C., and Lu, Z.: Using satellite observations to measure power plant emissions and their trends, *EM Magazine*, 64, 16–21, 2014.

Theys, N., Campion, R., Clarisse, L., Brenot, H., van Gent, J., Dils, B., Corradini, S., Merucci, L., Coheur, P.-F., Van Roozendaal, M., Hurtmans, D., Clerbaux, C., Tait, S., and Ferrucci, F.: Volcanic SO₂ fluxes derived from satellite data: a survey using OMI, GOME-2, IASI and MODIS, *Atmos. Chem. Phys.*, 13, 5945–5968, doi:10.5194/acp-13-5945-2013, 2013.

Tong, D. Q., Lamsal, L. N., Pan, L., Ding, C., Kim, H., Lee, P., Chai, T., Pickering, K. E., and Stajner, I.: Long-term NO_x trends over large cities in the United States during the Great Recession: comparison of satellite retrievals, ground observations, and emission inventories, *Atmos. Environ.*, 107, 70–84, 2015.

USEPA: Evaluating the Uncertainty of Emission Estimates, Vol. VI, Chapt. 4, Research Triangle Park, North Carolina, USA, 1996.

Valin, L. C., Russell, A. R., and Cohen, R. C.: Variations of OH radical in an urban plume inferred from NO₂ column measurements, *Geophys. Res. Lett.*, 40, 1856–1860, 2013.

van der A, R. J., Eskes, H. J., Boersma, K. F., van Noije, T. P. C., Van Roozendaal, M., De Smedt, I., Peters, D. H. M. U., and Meijer, E. W.: Trends, seasonal variability and dominant NO_x source derived from a ten year record of NO₂ measured from space, *J. Geophys. Res.*, 113, D04302, doi:10.1029/2007jd009021, 2008.

**Estimation of US
urban NO_x emissions
from OMI**

Z. Lu et al.

[Title Page](#)[Abstract](#)[Introduction](#)[Conclusions](#)[References](#)[Tables](#)[Figures](#)[Back](#)[Close](#)[Full Screen / Esc](#)[Printer-friendly Version](#)[Interactive Discussion](#)

- Veefkind, J. P., Aben, I., McMullan, K., Forster, H., de Vries, J., Otter, G., Claas, J., Eskes, H. J., de Haan, J. F., Kleipool, Q., van Weele, M., Hasekamp, O., Hoogeveen, R., Landgraf, J., Snel, R., Tol, P., Ingmann, P., Voors, R., Kruizinga, B., Vink, R., Visser, H., and Levelt, P. F.: TROPOMI on the ESA Sentinel-5 Precursor: a GMES mission for global observations of the atmospheric composition for climate, air quality and ozone layer applications, *Remote Sens. Environ.*, 120, 70–83, 2012.
- Wang, S. W., Streets, D. G., Zhang, Q. A., He, K. B., Chen, D., Kang, S. C., Lu, Z., and Wang, Y. X.: Satellite detection and model verification of NO_x emissions from power plants in northern China, *Environ. Res. Lett.*, 5, 044007, doi:10.1088/1748-9326/5/4/044007, 2010.
- Wang, S. W., Zhang, Q., Streets, D. G., He, K. B., Martin, R. V., Lamsal, L. N., Chen, D., Lei, Y., and Lu, Z.: Growth in NO_x emissions from power plants in China: bottom-up estimates and satellite observations, *Atmos. Chem. Phys.*, 12, 4429–4447, doi:10.5194/acp-12-4429-2012, 2012.
- Xing, J., Pleim, J., Mathur, R., Pouliot, G., Hogrefe, C., Gan, C.-M., and Wei, C.: Historical gaseous and primary aerosol emissions in the United States from 1990 to 2010, *Atmos. Chem. Phys.*, 13, 7531–7549, doi:10.5194/acp-13-7531-2013, 2013.
- Zhang, Q., Streets, D. G., and He, K. B.: Satellite observations of recent power plant construction in Inner Mongolia, China, *Geophys. Res. Lett.*, 36, L15809, doi:10.1029/2009gl038984, 2009.

Estimation of US urban NO_x emissions from OMI

Z. Lu et al.

Table 1. Summary of the average bottom-up NO_x emissions, OMI-derived NO_x results, ground-based NO₂ measurements, and their linear trends for 35 US urban areas during the summer half-year (April to September) from 2006* to 2013*.^a

Urban Areas	Latitude	Longitude	NEI emissions 2005–2014 (Mgh ⁻¹)	Results at high wind speeds (WS)			Results at low WS		Linear trends from 2006* to 2013* (%yr ⁻¹)			Mean R ^b	
				Mean WS (ms ⁻¹)	OMI-derived emissions (Mgh ⁻¹)	Effective lifetime (h)	Mean WS (ms ⁻¹)	OMI burden (Mg)	NEI emissions	OMI-derived emissions	OMI burden at WS < 3 ms ⁻¹		AQS
Atlanta, GA	33.74	-84.32	12.7	5.7	6.7±2.8	4.3±1.4	1.9	25.0±10.1	-7.9	-7.8±3.3	-15.3±6.2	-5.0	0.80
Boston, MA	42.38	-71.02	10.3	6.1	10.9±4.5	5.3±1.7	1.9	29.5±11.9	-6.1	-13.4±5.6	-8.1±3.3	-4.7	0.84
Charlotte, NC	35.34	-80.86	3.3	5.8	2.7±1.1	4.0±1.3	1.8	8.7±3.5	-1.3	-7.9±3.4	-12.9±5.2	-6.1	0.54
Chicago, IL	41.78	-87.68	30.7	7.4	23.3±9.7	6.1±1.9	2.1	86.3±34.8	-6.6	-7.8±3.3	-5.7±2.3	-6.8	0.95
Cincinnati, OH	39.12	-84.50	7.9	4.9	4.9±2.0	5.6±1.8	1.8	16.9±6.8	-3.9	-8.5±3.6	-6.0±2.5	-6.0	0.73
Dallas, TX	32.86	-96.96	14.8	7.4	8.1±3.4	3.3±1.1	2.0	26.8±10.8	-7.4	-12.2±5.1	-5.3±2.1	-7.3	0.86
Denver, CO	39.78	-105.04	10.0	6.0	12.1±5.0	3.5±1.1	1.8	21.7±8.6	-2.4	-9.8±4.1	-9.4±3.8	-2.1	0.78
Detroit, MI	42.26	-83.12	26.1	6.4	18.7±7.8	5.2±1.7	2.0	57.7±23.3	-6.6	-3.4±1.5	-5.8±2.3	-5.3	0.76
El Paso, TX	31.74	-106.38	2.2	6.7	3.2±1.3	3.0±0.9	1.9	7.2±2.9	-3.3	-3.7±1.6	-4.4±1.8	-4.6	0.77
Houston, TX	29.82	-95.28	13.5	5.9	11.3±4.7	4.1±1.3	1.9	30.3±12.2	-7.9	-5.2±2.3	-5.1±2.1	-4.8	0.79
Indianapolis, IN	39.80	-86.12	4.3	5.6	3.1±1.3	4.2±1.3	2.0	8.5±3.4	-3.2	-5.7±2.5	-6.5±2.6	-7.8	0.86
Jacksonville, FL	30.40	-81.60	5.2	5.7	4.7±2.0	2.5±0.8	1.9	9.9±4.0	-9.5	-6.3±2.8	-9.5±3.8	-2.9	0.80
Kansas City, MO	39.10	-94.56	10.2	6.6	5.1±2.1	3.9±1.2	1.9	14.3±5.8	-4.4	-7.8±3.3	-13.4±5.4	-4.9	0.86
Las Vegas, NV	36.18	-115.14	6.1	6.4	6.7±2.8	2.0±0.7	1.9	11.2±4.5	-3.3	-10.3±4.4	-12.3±5.0	-3.0	0.60
Los Angeles, CA	34.06	-117.92	40.1	3.7	40.0±16.6	3.6±1.2	2.0	124.4±45.2	-10.7	-7.0±2.9	-8.5±3.4	-7.6	0.97
Louisville, KY	38.20	-85.74	6.3	5.6	2.5±1.0	3.5±1.1	1.9	8.1±3.3	-7.6	-9.0±3.8	-11.3±4.6	-13.1	0.70
Memphis, TN	35.10	-90.04	4.4	5.9	1.5±0.6	3.2±1.0	1.9	3.4±1.4	-7.3	-25.9±10.8	-10.2±4.1	-2.7	0.83
Miami, FL	26.02	-80.34	13.4	5.4	5.6±2.3	5.0±1.6	1.9	28.7±11.6	-6.5	-10.2±4.3	-4.5±1.8	-9.3	0.80
Minneapolis, MN	44.96	-93.22	12.8	6.9	9.3±3.9	2.7±0.9	2.0	25.9±10.5	-8.6	-12.4±5.2	-11.3±4.6	-11.0	0.89
Nashville, TN	36.14	-86.62	2.9	5.6	2.0±0.8	2.8±0.9	1.8	4.0±1.6	-4.4	-13.8±5.8	-14.9±6.0	-6.9	0.78
New Orleans, LA	29.98	-90.22	7.2	5.3	3.6±1.5	3.2±1.0	1.8	6.0±2.5	-5.2	-7.3±3.2	-1.8±1.1	-5.4	0.48
New York, NY	40.72	-73.80	43.2	5.3	50.7±21.1	3.1±1.0	1.9	128.1±51.7	-6.3	-5.9±2.5	-6.8±2.8	-6.7	0.96
Philadelphia, PA	39.98	-75.16	17.8	5.2	23.3±9.8	3.2±1.0	1.9	53.0±21.4	-7.2	-9.1±4.0	-18.1±7.3	-7.2	0.93
Phoenix, AZ	33.54	-112.00	10.8	5.4	12.2±5.1	1.8±0.6	1.7	21.1±8.5	-4.7	-13.0±5.5	-6.4±2.6	-4.6	0.80
Portland, OR	45.44	-122.60	6.9	3.9	9.9±4.1	1.2±0.4	2.1	15.8±6.4	-3.8	-5.0±2.2	-11.6±4.7	-8.1	0.91
Richmond, VA	37.42	-77.30	3.6	4.9	1.8±0.7	3.5±1.1	2.0	5.1±2.1	-7.8	-5.7±2.7	-14.7±5.9	-9.4	0.68
Salt Lake City, UT	40.72	-111.92	3.6	4.8	8.2±3.5	1.3±0.4	1.8	14.3±5.8	-3.7	-12.1±5.4	-9.3±3.8	-10.8	0.89
San Antonio, TX	29.56	-98.44	5.4	5.7	3.2±1.4	2.1±0.7	2.0	7.9±3.2	-5.7	-10.2±4.4	-8.2±3.4	-1.6	0.75
San Diego, CA	32.66	-116.86	6.0	4.0	8.8±3.7	3.1±1.0	2.0	21.7±8.8	-9.8	-6.3±3.0	-4.2±1.7	-7.8	0.91
Seattle, WA	47.42	-122.22	13.0	3.7	13.3±5.7	3.4±1.1	2.0	30.0±12.1	-4.8	-6.5±3.3	-4.3±1.9	-5.6	0.80
St. Louis, MO	38.64	-90.32	11.0	5.2	4.9±2.0	6.8±2.1	1.9	15.8±6.4	-0.7	-10.9±4.5	-8.9±3.6	-10.0	0.59
Tampa, FL	27.90	-82.42	8.5	5.6	6.9±2.9	2.7±0.9	1.8	14.3±5.8	-9.5	-6.6±2.8	-9.1±3.7	-10.5	0.80
Tucson, AZ	32.24	-110.88	3.1	5.9	1.5±0.6	3.6±1.2	1.8	3.9±1.6	-6.0	-6.2±2.7	-4.0±1.7	-7.4	0.59
Virginia Beach, VA	36.90	-76.32	6.1	6.2	4.6±1.9	1.4±0.4	2.0	7.3±2.9	-8.7	-8.9±3.7	-8.7±3.5	-6.1	0.79
Washington, DC	39.20	-76.58	18.5	5.0	13.0±5.5	4.7±1.5	1.9	48.5±19.6	-7.3	-10.2±4.3	-6.9±2.8	-6.2	0.92

^a 2006* and 2013* denote the three-year average of 2005–2007 and 2012–2014, respectively.

^b Average correlation coefficients (R) of pair-wise trends among the NEI NO_x emissions, the OMI-derived NO_x emissions, the OMI NO₂ burdens, and the AQS NO₂ measurements.

Title Page

Abstract Introduction

Conclusions References

Tables Figures

◀ ▶

◀ ▶

Back Close

Full Screen / Esc

Printer-friendly Version

Interactive Discussion



Estimation of US urban NO_x emissions from OMI

Z. Lu et al.

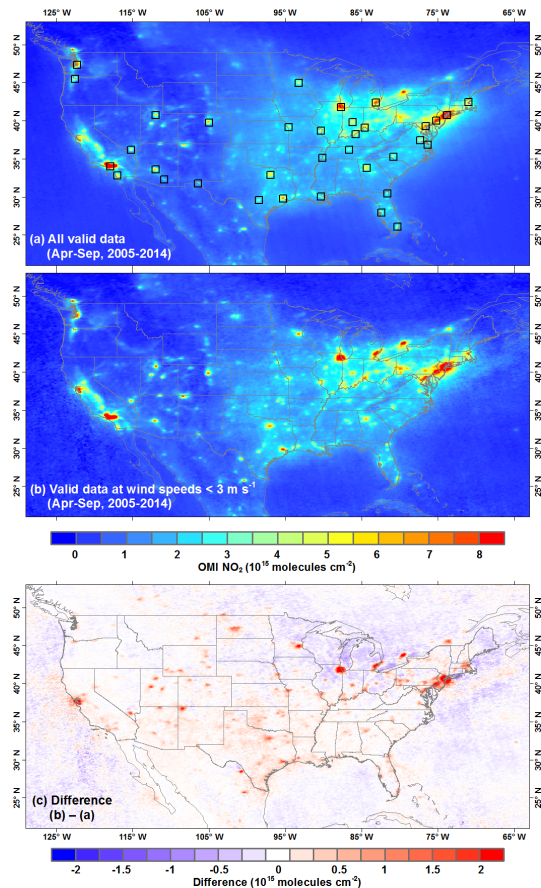


Figure 1. Average summer half-year (i.e., April to September) OMI NO₂ TVCDs over the continental US during 2005–2014: **(a)** all valid data were used, **(b)** only valid data with wind speeds < 3 ms⁻¹ were used, and **(c)** the difference between **(b)** and **(a)**. Squares in **(a)** indicate the urban areas selected in this work.

Title Page

Abstract

Introduction

Conclusions

References

Tables

Figures



Back

Close

Full Screen / Esc

Printer-friendly Version

Interactive Discussion



Estimation of US urban NO_x emissions from OMI

Z. Lu et al.

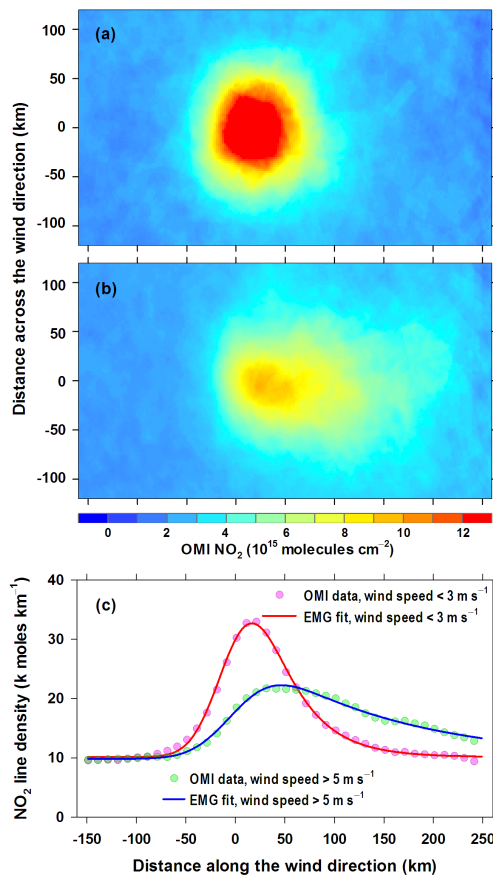


Figure 2. Wind-aligned OMI NO₂ TVCD maps at wind speeds **(a)** <math>< 3 \text{ m s}^{-1}</math> and **(b)** > 5 m s⁻¹ for Chicago in summer months (i.e., April to September) during 2005–2007. **(c)** OMI NO₂ line densities of **(a)** and **(b)** and the corresponding EMG fits. Line densities are from the integration of the NO₂ data in the across-wind direction.

Estimation of US urban NO_x emissions from OMI

Z. Lu et al.

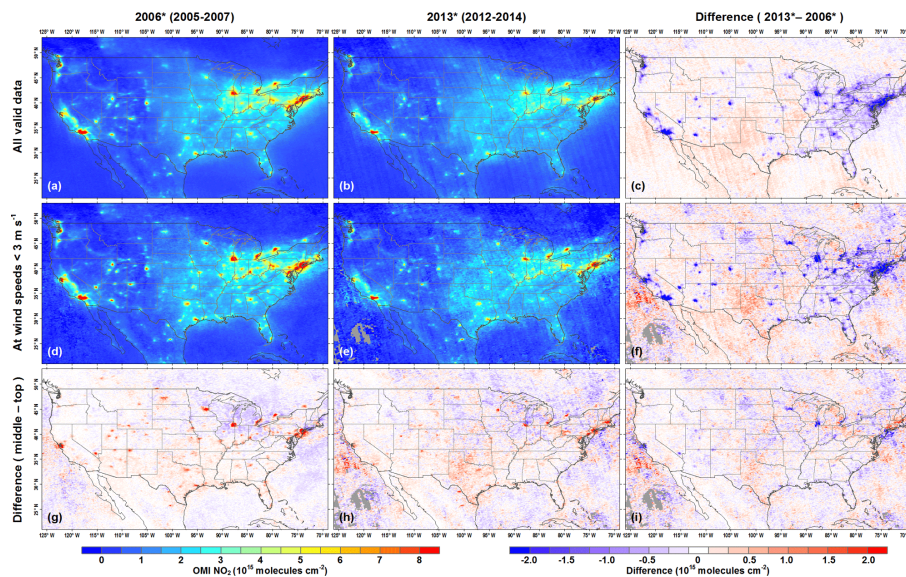


Figure 3. Average summer half-year (i.e., April to September) OMI NO₂ TVCDs over the continental US for (a, d) 2006* (i.e., 2005 to 2007) and (b, e) 2013* (i.e., 2012 to 2014): (a, b) all valid data were used, (d, e) only valid data with wind speeds $< 3 \text{ ms}^{-1}$ were used. The right column shows the differences in maps between the middle and the left column. The bottom row shows the differences in maps between the middle and the top row.

Title Page

Abstract

Introduction

Conclusions

References

Tables

Figures



Back

Close

Full Screen / Esc

Printer-friendly Version

Interactive Discussion



Estimation of US urban NO_x emissions from OMI

Z. Lu et al.

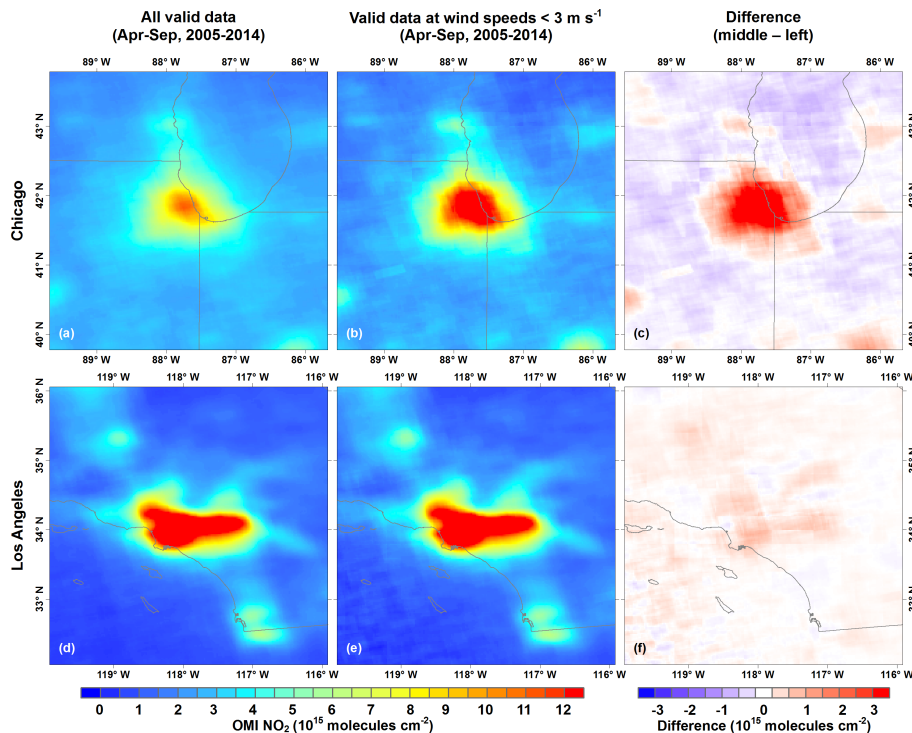


Figure 4. Average summer half-year (i.e., April to September) OMI NO₂ TVCDs over (a, b) Chicago and (d, e) Los Angeles during 2005–2014: (a, d) all valid data were used, (b, e) only valid data with wind speeds < 3 m s⁻¹ were used, and (c, f) the difference between the middle and the left column.

Title Page

Abstract

Introduction

Conclusions

References

Tables

Figures



Back

Close

Full Screen / Esc

Printer-friendly Version

Interactive Discussion



Estimation of US urban NO_x emissions from OMI

Z. Lu et al.

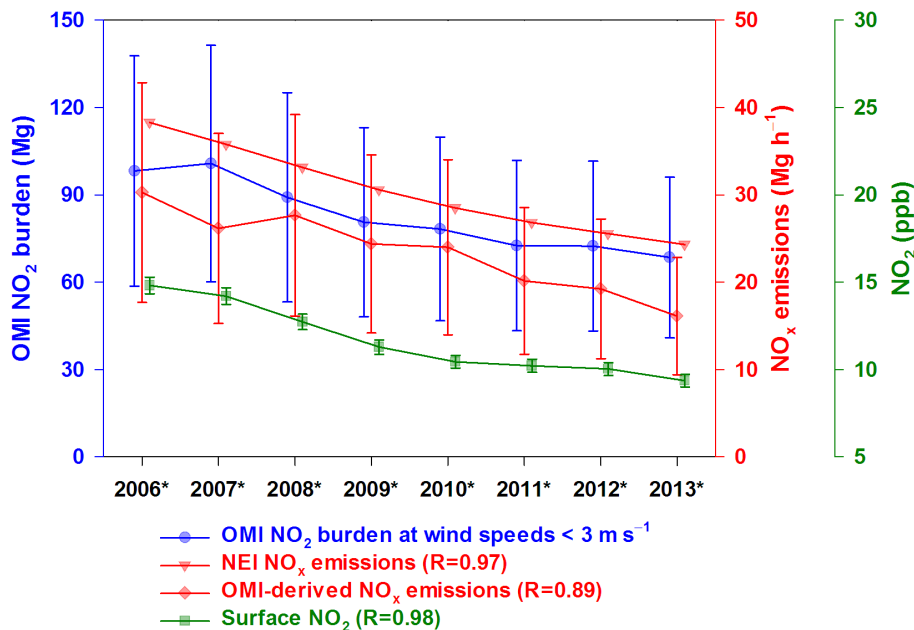


Figure 5. Interannual trends of NEI NO_x emissions, the OMI-derived summertime (April to September) NO_x emissions, the OMI-observed summertime NO₂ burdens at low (< 3 m s⁻¹) speed winds condition, and the average summertime NO₂ concentrations at 13:00–14:00 LT in Chicago during 2006*–2013*. Error bars express the ±1 SD uncertainties. *R* values shown are the correlation coefficients with the OMI-observed NO₂ burdens.

Estimation of US urban NO_x emissions from OMI

Z. Lu et al.

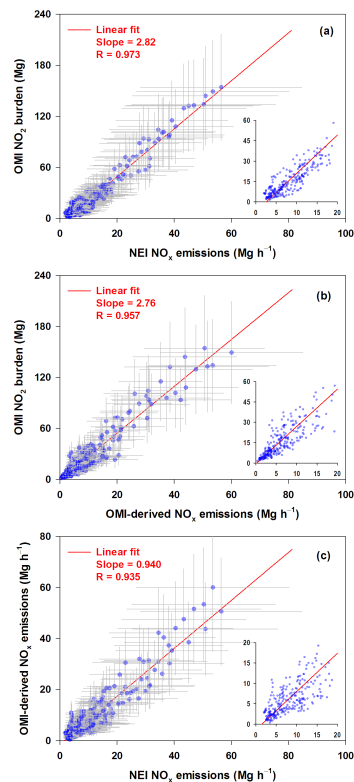


Figure 6. Scatter plots of (a) OMI-observed NO₂ burdens at low ($< 3 \text{ ms}^{-1}$) speed winds condition against NEI NO_x emissions, (b) OMI-observed NO₂ burdens against OMI-derived NO_x emissions, and (c) OMI-derived NO_x emissions against NEI NO_x emissions for 35 selected US urban areas during 2005–2014. Each point represents a three-year result for an urban area. Error bars express the ± 1 SD uncertainties. Uncertainties of NEI emissions are set to be 50% according to the expert judgment. The inset figures are the zoomed views of points with emissions $< 20 \text{ Mg h}^{-1}$.

[Title Page](#)[Abstract](#)[Introduction](#)[Conclusions](#)[References](#)[Tables](#)[Figures](#)[Back](#)[Close](#)[Full Screen / Esc](#)[Printer-friendly Version](#)[Interactive Discussion](#)

Estimation of US urban NO_x emissions from OMI

Z. Lu et al.

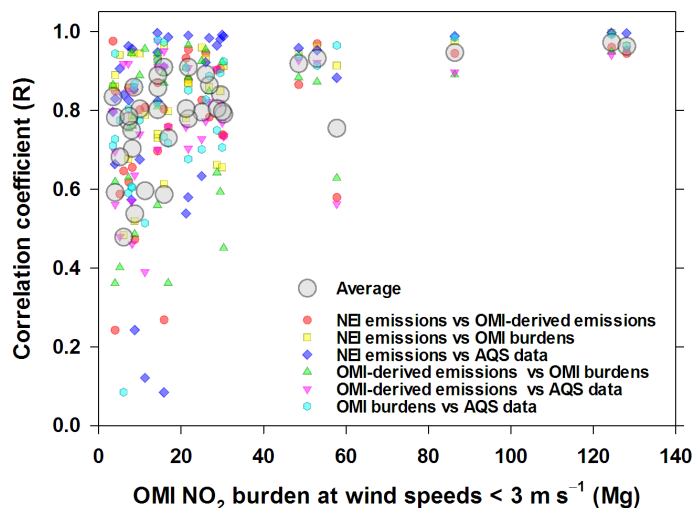


Figure 7. Correlation coefficients of pair-wise trends among the NEI NO_x emissions, the OMI-derived NO_x emissions, the OMI NO₂ burdens at wind speeds < 3 m s⁻¹, and the AQS NO₂ measurements against the mean OMI NO₂ burdens under the weak-wind speed condition (< 3 m s⁻¹) for all selected urban areas during 2006*–2013*. Each large grey circle represents the average of the six correlation coefficients for an urban area.

Title Page

Abstract

Introduction

Conclusions

References

Tables

Figures



Back

Close

Full Screen / Esc

Printer-friendly Version

Interactive Discussion



Estimation of US urban NO_x emissions from OMI

Z. Lu et al.

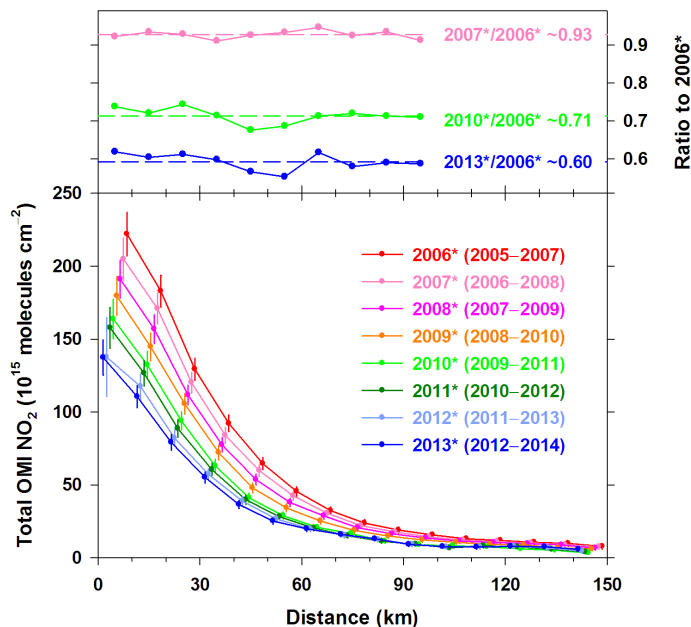


Figure 8. The sum of three-year averaged OMI NO₂ TVCDs under the weak-wind speed condition for 35 selected US urban areas as a function of the distance from the urban centers during 2006* to 2013*. The background NO₂ of urban areas was removed. Error bars express the 95 % confidence intervals of the mean. The ratios of 2007* to 2006*, 2010* to 2006*, and 2013* to 2006* are shown at the top.

Title Page

Abstract

Introduction

Conclusions

References

Tables

Figures

◀

▶

◀

▶

Back

Close

Full Screen / Esc

Printer-friendly Version

Interactive Discussion



Estimation of US urban NO_x emissions from OMI

Z. Lu et al.

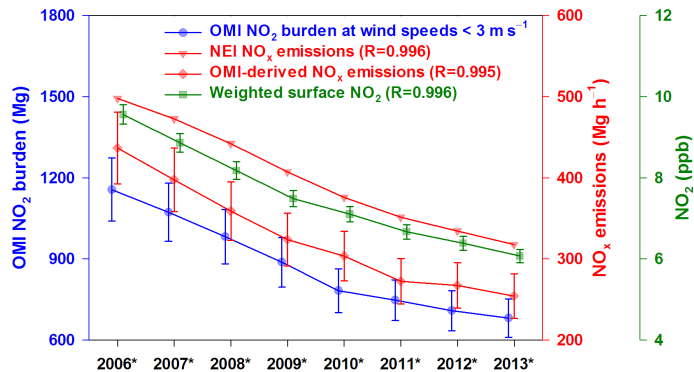


Figure 9. Three-year moving trends of the total NEI NO_x emissions, the total OMI-derived NO_x emissions, the total OMI-observed NO₂ burdens under the weak-wind speed condition, and the area-weighted average AQS surface NO₂ measurements for all selected urban areas during 2006*–2013*. Error bars express the ± 1 SD of the estimates. R values shown are the correlation coefficients with the OMI-observed NO₂ burdens.